nature astronomy

Article

https://doi.org/10.1038/s41550-023-02012-x

Hydrothermal fluid activity on asteroid Itokawa

In the format provided by the authors and unedited

Table of Contents

Supplementary Text

Random distribution of NaCl in the Itokawa plagioclase

It is well-known that plagioclase can develop perfect cleavage systems[51]. Therefore, it is intuitive to speculate that NaCl grains should form preferentially along cleavage planes of the Itokawa plagioclase. However, there are multiple reasons why NaCl shows a random distribution pattern and is associated with an irregular alteration vein in our sample. First, the fact that plagioclase can develop perfect cleavage systems does not mean that any fractures in plagioclase should necessarily follow cleavage planes. It is well documented in the literature that both terrestrial and extraterrestrial plagioclase can contain irregular fractures and alteration veins which do not follow cleavage planes[52–57]. Studies of shock metamorphism of chondrites also show that plagioclase can form irregular fractures during shock events[58,59]. Irregular fractures and alteration veins were also reported in other minerals that have perfect cleavage (such as calcite[60–63]). Second, pores and fractures generated in minerals during fluid alteration do not necessarily show preferred orientation. Mineral-fluid interactions are controlled by coupled dissolution and precipitation which can generate pores for fluids to penetrate into the interior of minerals[62,64]. Such pores can further develop into interconnected pathways or fractures with increasing degrees of alteration[62,65,66]. Based on these previous studies, the formation and distribution of pores and fractures are controlled by multiple factors, such as the relative solubility of parent and product phases, and the local fluid chemistry at the mineral-fluid interfaces. Even in minerals that can develop perfect cleavage systems (e.g., calcite and plagioclase), the distribution of pores and fractures is commonly not correlated with cleavage planes. Third, in meteorites, random distribution of fluid inclusions was previously observed in halite and calcite[67,68], both of which can develop perfect cleavages. This observation further proves that the distribution of fluid inclusions and their precipitates is not controlled by the cleavage systems.

Comparison between Itokawa particles, Monahans and Zag

The two equilibrated ordinary chondrites (OCs) Monahans and Zag contain abundant halite crystals, some of which enclose micrometer-sized fluid inclusions[69,70]. In comparison, no such fluid inclusions were previously reported in Itokawa particles. The lack of fluid inclusions could be simply attributed to the fact that NaCl grains in the particle RA-QD02-0248 are only a few hundred nanometers at most and therefore could not incorporate fluid inclusions. An alternative explanation is that the nanometer-sized NaCl crystals in RA-QD02-0248 could represent crystallization products of fluid trapped in pores during the formation of albitic plagioclase, as we discussed in in the Discussion section.

Zolensky and co-authors[69] did cooling experiments on the fluid inclusions in Monahans and Zag, and based on the rarity of vapor bubbles in the fluid inclusions, they suggested a low formation temperature of probably <50 °C. These authors further suggested that halite grains in Monahans and Zag are exogenous and formed on a carbonaceous parent body. Halite formed in this way is not expected to show textural relationships with other secondary phases that are indigenous to OCs, which is different from our textural observations of RA-QD02-0248. In addition, the intimate textural association between NaCl and plagioclase in RA-QD02-0248 indicates in-situ formation of NaCl. Therefore, the conditions under which halite fluid inclusions in Monahans and Zag formed may not be directly applied to Itokawa particles. It is possible that Monahans and Zag may have experienced a different alteration history from Itokawa particles. Alternatively, there might be a potential caveat in the temperature constraints from the fluid inclusions in Monahans and Zag: vapor bubbles that were initially present in the fluid inclusions could have leaked before the fall of the meteorites. The in-situ formation of halite in Monahans and Zag is supported by the I-Xe dating of Zag halite[71] which suggested an early formation prior

to the disruption of the H chondrite parent body. Additionally, a very recent U-Pb and REE study of apatite in Zag[72] suggested that halite in Zag formed early on the parent body via precipitation from a fluid. Therefore, there is a possibility that halite in Monahans and Zag formed in situ, in a similar way to the formation of NaCl grains in RA-QD02-0248. However, a definitive explanation for the difference between Monahans, Zag, and Itokawa particles requires a systematic and detailed investigation into the petrology and mineralogy of Monahans and Zag, which is beyond the scope of this study. A textural association relationship between halite and other secondary phases in Monahans and Zag would argue for an in-situ origin of halite.

Source of the NaCl-forming brine on Itokawa

The brine that precipitated NaCl in Itokawa particles could be indigenous. Based on thermodynamic modeling[73], HCl could condense as HCl hydrate ($HCl{\cdot}3H_2O$) at ~160-140 K in the early solar nebula. This HCl condensate then accreted with water ice into the parent bodies of chondrites and was later melted by the decay of short-lived radionuclides to produce a low-pH aqueous solution. Therefore, the HCl hydrate could serve as a potential source of Cl in chondritic asteroids. Chondrule mesostases might also contribute Cl to the aqueous fluid. However, it is still unclear if mesostases in ordinary chondrites (OCs) contained primary Cl[53]. With progressive water-rock interactions, the aqueous fluid could become concentrated in alkali elements and halogens and precipitate salt crystals. This alteration scenario is consistent with our proposed alteration mechanism of NaCl in RA-QD02-0248. Rubin et al.[70] proposed a similar origin for halites in Monahans and Zag; however, different from our proposed mechanism, these authors suggested that the halite-forming brine was released by late-stage impact events that dehydrated phyllosilicates. In their scenario, the resulting aqueous fluid percolated through the cold regolith of OC parent bodies and eventually precipitated halite in Monahans and Zag. There are potential issues with this origin of brine. First, if the aqueous fluid was derived from the cold regions of the asteroids, it could produce other hydrous phases (e.g., phyllosilicates) that are stable at relatively low temperatures. However, such phases are not observed in Monahans, Zag, and Itokawa particles. Second, dehydration of phyllosilicates is unlikely to produce large-scale flow of aqueous fluid that could percolate through the regolith and precipitate abundant halite grains in Monahans and Zag. Fluid flow, even in parent bodies of more hydrated carbonaceous chondrites, was very limited[74]. The limited fluid flow is also consistent with the isochemical nature of alteration reactions in bulk carbonaceous and ordinary chondrites[2].

Another possible source of brine is degassing of partial melts in the asteroid core or impact generated melts during retrograde metamorphism[75,76]. The parent asteroids of chondrites might have preserved a partially melted and differentiated interior due to the heating of short-lived radiogenic isotopes[77–79]. Volatiles in the interior could migrate as supercritical fluids to the chondritic crusts via buoyancy-driven Darcy flow[80,81]. Progressive interactions between such a fluid and phosphates in a crust with OC compositions during the fluid ascent could produce a Cl-rich fluid at lower depths due to strong partitioning of F into apatite[75,76]. Similarly, degassing of localized impact melts might release a briny fluid[75,76]. The brine formed by degassing was proposed to be responsible for the formation of K-rich feldspars and some Cl-rich apatites in OCs[54,76,82]. Fine-scale exsolution lamellae and patches of K-feldspar are commonly observed in albitic plagioclase in type 3.6 to 6 OCs and are restricted to the grain edges of albite[83]. Because the interdiffusion rates of Na and K in alkali feldspars are rapid at the inferred peak metamorphic conditions of OCs[84,85], Jones and co-workers[54,76,82] concluded that K was likely incorporated into plagioclase by a H_2O-poor fluid during retrograde metamorphism. However, our TEM observations are not consistent with this alteration scenario. In our FIB sections, NaCl grains do not show any textural relationship with K-feldspar exsolution lamellae but are instead randomly dispersed in plagioclase. This relationship is best illustrated by Section #3, where K-rich lamellae that formed by spinodal decomposition are restricted to a ~500 nm wide region along the grain boundary. If NaCl precipitated from the same anhydrous

fluid that introduced K into plagioclase, these salt crystals would be expected to be present mainly adjacent to the grain boundary in Section #3. This decoupling between NaCl precipitation and K incorporation is further supported by the lack of K enrichment of the alteration vein in Section #5. Therefore, to reconcile the timing of NaCl formation with retrograde metamorphism, we hypothesize that at least two fluid events are necessary: one introducing K into plagioclase and later another one producing NaCl. Because NaCl grains have a random distribution in plagioclase, the latter fluid must have penetrated further into plagioclase crystals, compared with the K-enriched fluid. Although we cannot exclude this multi-stage alteration scenario, there is currently no obvious evidence for multiple late-stage anhydrous fluid events on OC parent bodies.

There is also a possibility that the NaCl-forming brine is exogeneous. Several previous studies[67,69,86–88] proposed that halites in Monahans and Zag represent a clastic component delivered into the asteroid surface from a large, carbonaceous, aqueously active body, such as Ceres. This hypothesis is based on: (1) halite is exceptionally rare in chondrites; (2) a CI-like clast with halite is present in Zag; (3) salt crystals are associated with the current cryovolcanism on Enceladus; (4) fluid inclusions within the Monahans and Zag halites are far from equilibrium, similar to cryovolcanic fluids on Enceladus; (5) H isotopes of the Monahans and Zag fluid inclusions are comparable to hydrovolcanic fluids on Enceladus today. Halite formed in this way is not expected to show textural association with other secondary phases (e.g., such as albitic plagioclase) as we observed in RA-QD02-0248. Therefore, our data suggest that an indigenous hydrothermal fluid as the brine source is most compatible with the textural observations of the Itokawa particle RA-QD02-0248.

Additional implications for fluid alteration on OC parent bodies

OCs show a different fluid alteration style from carbonaceous chondrites (CCs). For example, in OCs, albitization of plagioclase is widespread and mobility of Al is significantly enhanced with the formation of leached chondrules (see review by reference [52]). NaCl in the Itokawa particle potentially provides an additional insight into the causes of the different alteration styles. NaCl precipitated from a high-temperature, alkali-halogen-rich, hydrothermal fluid which was capable of producing widespread albitization and mobilizing Al. High-temperature fluid can significantly accelerate the reaction rates of albitization[89] and enhance the mobility of Al[90]. The higher temperature experienced by OCs than CCs could be a key factor in their different alteration styles. Previous thermodynamic models of chondrite alteration[91] predicted that NaCl could precipitate from fluids with high activity of NaCl, but NaCl with an unambiguous hydrothermal origin was never reported until the discovery of NaCl in the Itokawa particle. The hydrothermal origin of NaCl in the Itokawa particle is also consistent with the thermodynamic model[73] which suggested HCl hydrate ($HCl \cdot 3H_2O$) that condensed from the solar nebular gas could be a source of fluids on chondrite parent bodies: the distribution of HCl hydrate on the asteroids could control the initial fluid compositions and whether NaCl could form.

Before the recent H isotopic study of Itokawa pyroxene[92], only a few studies measured the water contents of ordinary chondrites. These studies showed that the water contents of OCs are typically <0.2 wt% which are significantly lower than those of CCs, e.g., ~20 wt% and ~9 wt% for CIs and CMs, respectively[93–96]. Most of these studies were conducted on type 3 OCs that did not experience significant thermal metamorphism. Some reasons for this lack of data include (1) equilibrated OCs were commonly assumed to be thermally metamorphosed in the absence of water[52], which was only recently challenged by the studies of plagioclase and phosphates[54,82,97,98]; and (2) equilibrated OCs were completely dehydrated due to intense thermal metamorphism[54], making detection of water in these samples very difficult. The paper by Jin and Bose[92] provided a new constraint on water content (160 to 510 ppm) of equilibrated OCs using Itokawa particle. Our study of NaCl provides further support for the high H_2O contents estimated by these authors, suggesting that the equilibrated OCs were indeed more hydrated than previously thought. The amount of water required to

produce NaCl can potentially be estimated quantitatively using solubility data of NaCl in water[99], but the size of the Itokawa particle we report on here precludes a reliable constraint because it represents a tiny portion of the original rock in which the abundances of different mineral phases (including NaCl) are unknown.

Supplementary Figs. 1-15

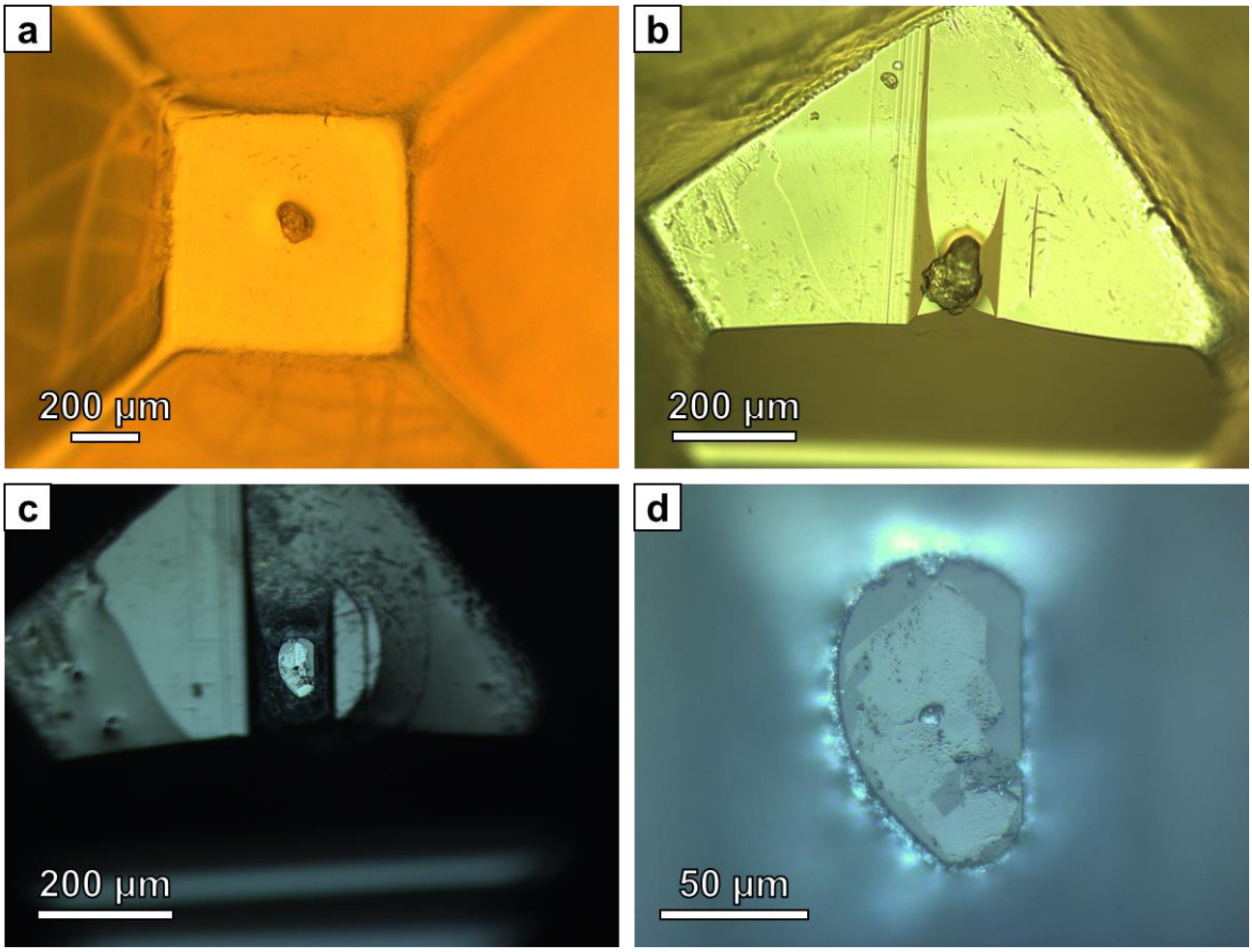

Supplementary Fig. 1 | Optical microscopy reflected light images illustrating the preparation procedure of the Itokawa particle RA-QD02-0248. (**a**) The particle was transported onto the top of an epoxy bullet. (**b**) The top of the epoxy bullet was trimmed to remove the epoxy material surrounding the particle and create a ~150 µm × 150 µm block that contains the particle. (**c**) The block was then sliced until a flat surface of the particle was exposed. (**d**) A higher-magnification image showing the flat surface of the particle after the final slicing.

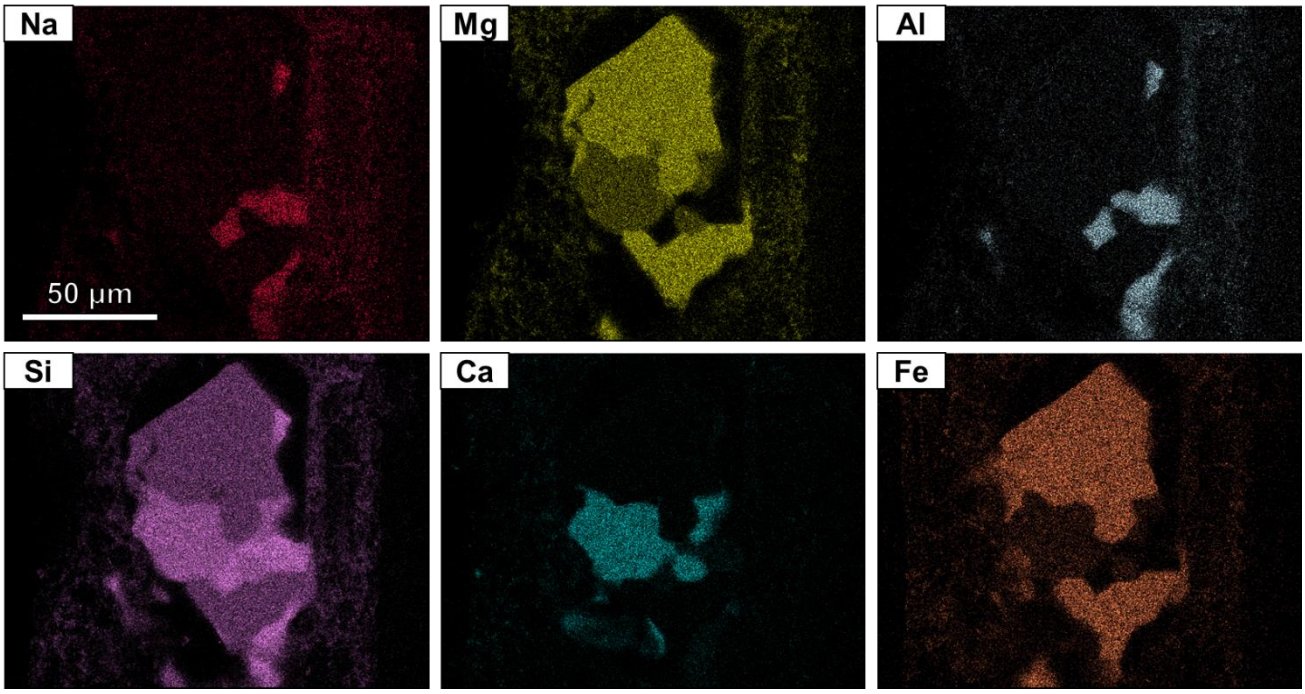

Supplementary Fig. 2 | EDS X-ray maps of RA-QD02-0248 that were collected on the Helios FIB-SEM. These maps were used to construct a phase map shown in supplementary Fig. 3.

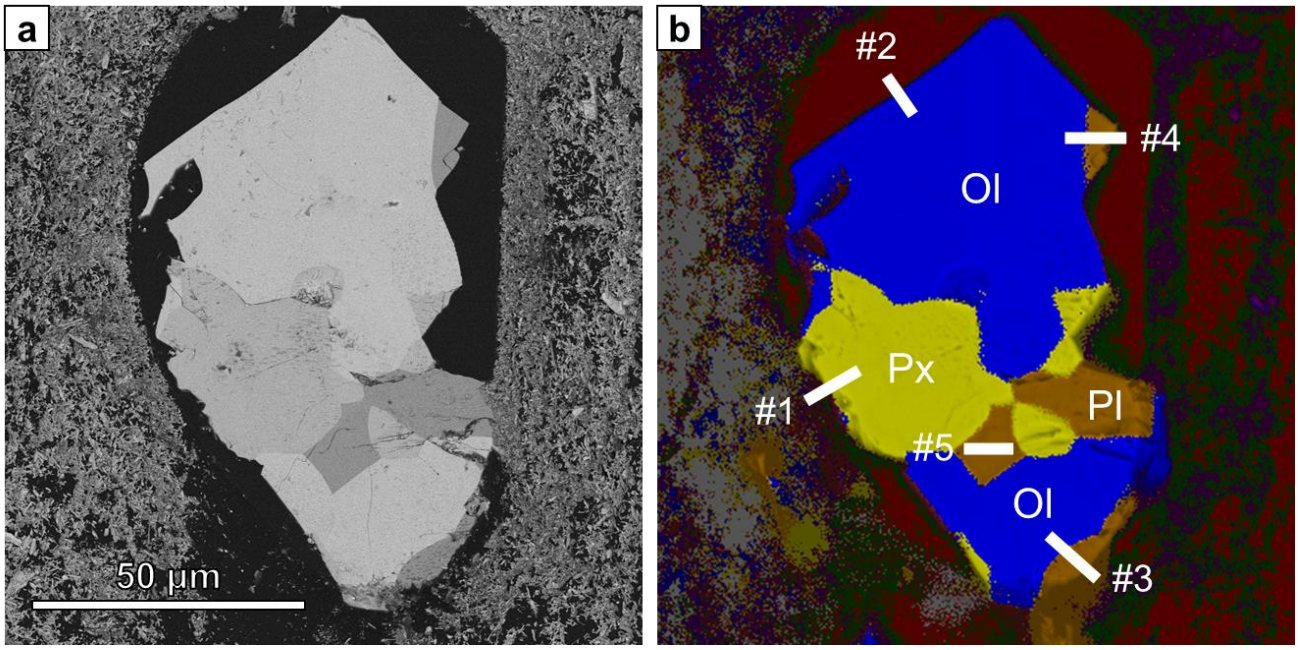

Supplementary Fig. 3 | Backscattered electron image (a) and phase map (b) of Itokawa particle RA-QD02-0248. The particle is composed of olivine (Ol), high-Ca pyroxene (Px), and plagioclase (Pl). The straight or slightly curved grain boundaries and triple junctions point to an equilibrated texture. The white stripes on the phase map correspond to the locations of FIB sections. Sections #3-5 that transect plagioclase are investigated in this study.

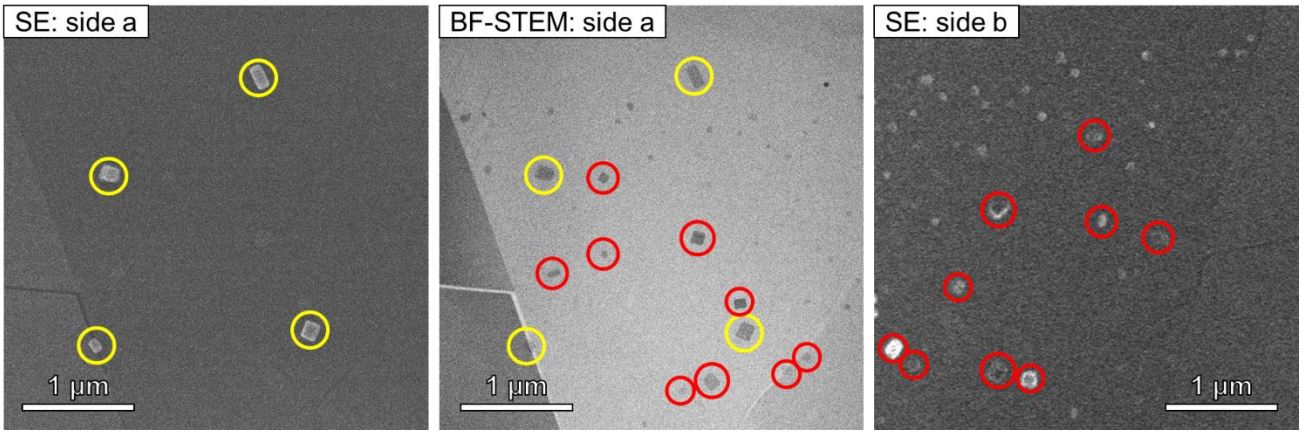

Supplementary Fig. 4 | SE and BF-STEM images of sides a and b of FIB section #3 are compared to reveal potential NaCl inclusions within the thickness of the FIB section. Yellow and red circles outline relatively large grains that occur on the surfaces of side a and b, respectively. All these grains are surface-adhering. We also counted the smaller grains: most occur on the surfaces, although the rest of the grains are too small to be clearly resolved on the images.

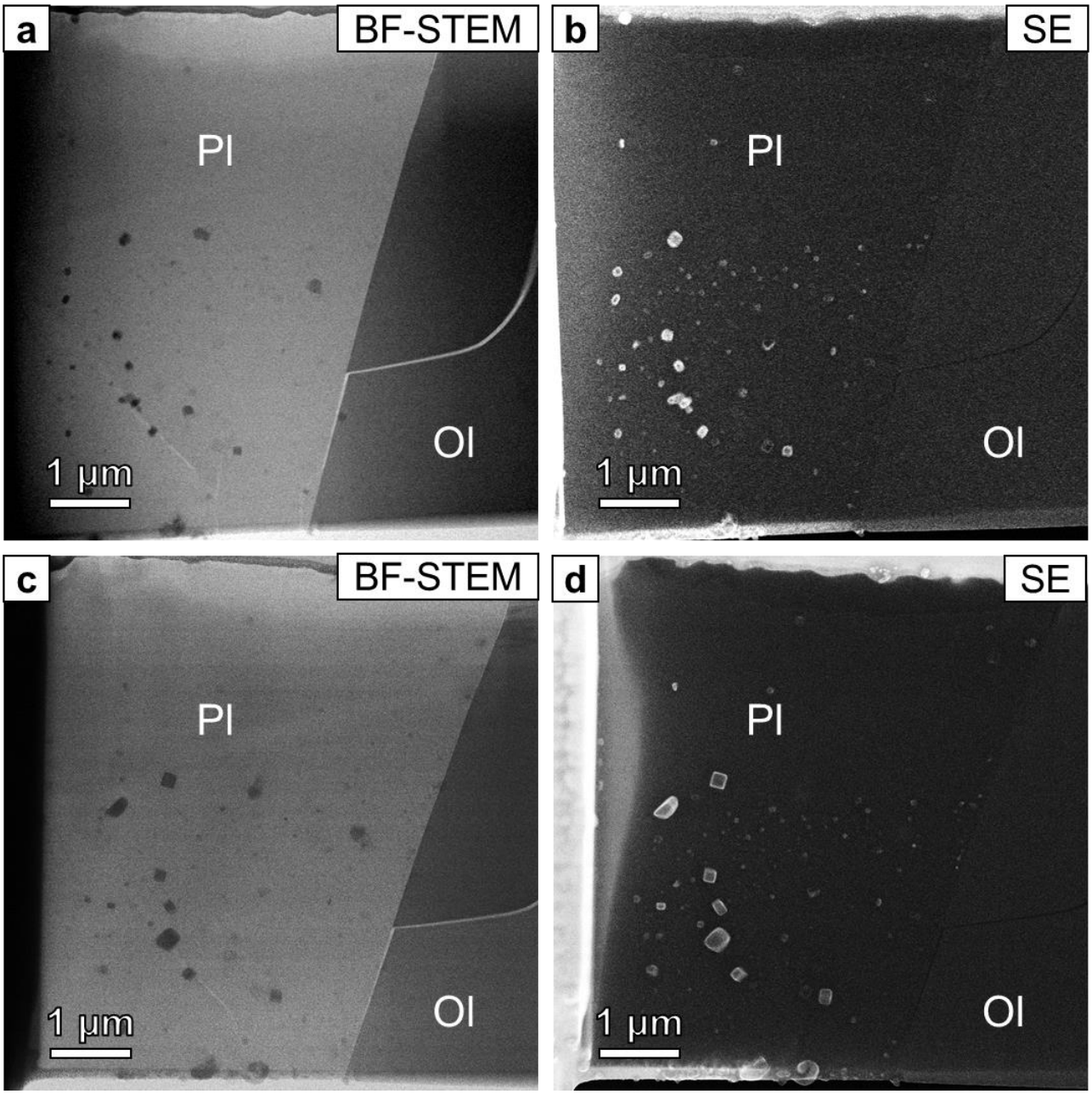

Supplementary Fig. 5 | Comparison of STEM images obtained in September 2016 (a-b) and September 2021 (c-d). The overall distribution of NaCl grains remained unchanged for five years. Minor changes to the sizes and shapes of some grains are observed, especially those >100 nm. Abbreviations: Ol, olivine; Pl, plagioclase.

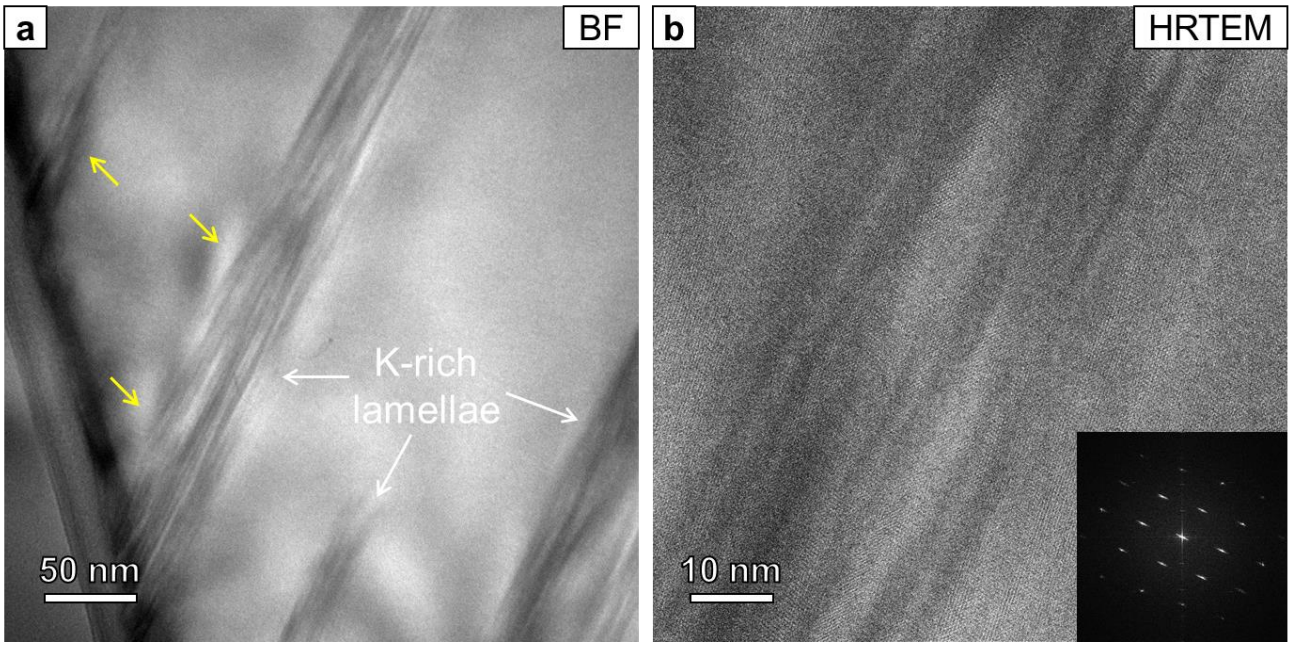

Supplementary Fig. 6 | BF-TEM and HRTEM images of FIB section #3 showing the presence of K-feldspar exsolution lamellae that formed by spinodal decomposition. (**a**) K-feldspar lamellae are extending from the plagioclase-olivine interface into plagioclase. The lamellae are composed of narrow spindles. Yellow arrows indicate coherency strains that developed during the Na^{+}-K^{+} interdiffusion in plagioclase. (**b**) The spindle-shaped lamella is better revealed by the HRTEM image. Also shown in the lower right corner is a Fast Fourier Transform pattern of the lamella. The presence of spindles produces streaking on the diffraction spots.

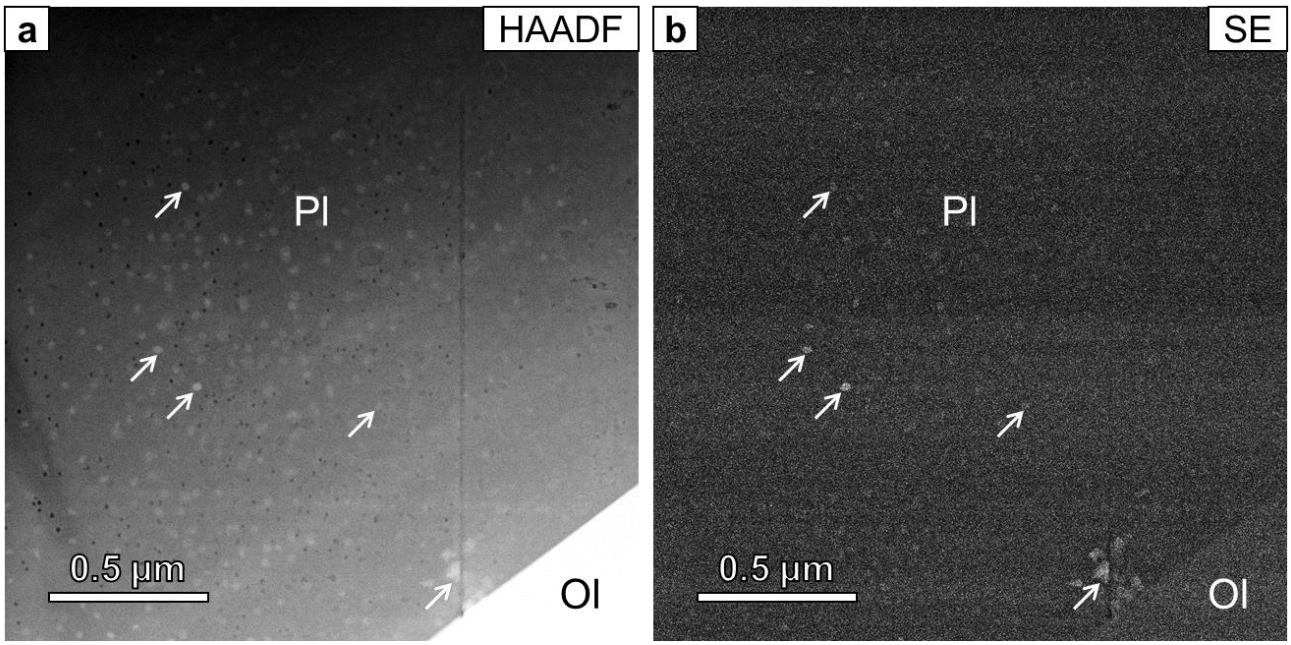

Supplementary Fig. 7 | HAADF and SE images of FIB section #4 showing that abundant fine-grained, high-Z phases are present on the surface of plagioclase (Pl). Some of these phases are indicated by the white arrows. No such phases are found on the adjacent olivine (Ol).

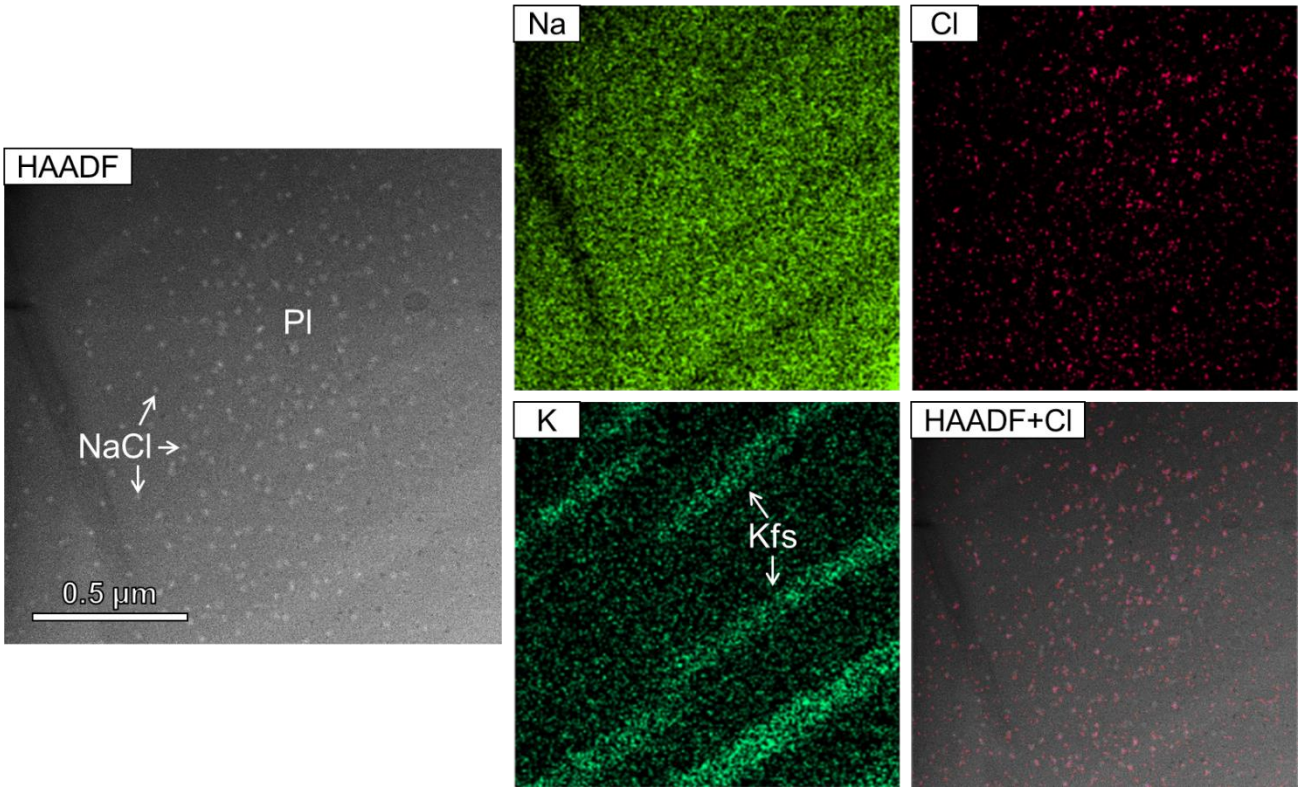

Supplementary Fig. 8 | HAADF image and corresponding EDS X-ray maps showing the distribution of fine-grained NaCl crystals on plagioclase (Pl) in FIB section #4. NaCl grains cannot be clearly resolved on the Na map due to their small sizes, but their presence is indicated by the hotspots on the Cl map. These Cl hotspots are associated with the high-Z phases on the HAADF image, as demonstrated by the bottom right image where Cl map (in red) is superimposed on the HAADF image. Plagioclase contains K-feldspar (Kfs) exsolution lamellae which do not show any textural relationship with NaCl grains.

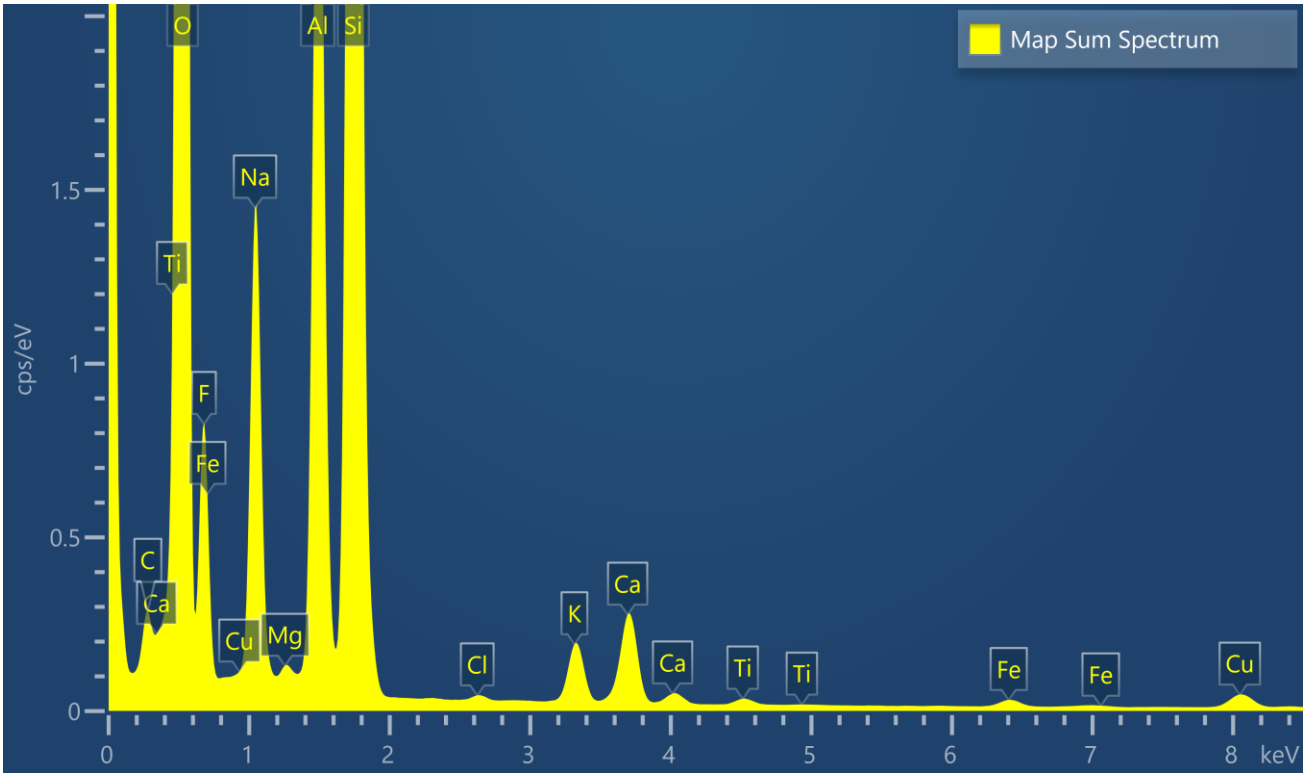

Supplementary Fig. 9 | The summed spectrum of the EDS X-ray maps shown in supplementary Fig. 7. A small Cl Kα peak is observed, and it is clearly resolved from the background.

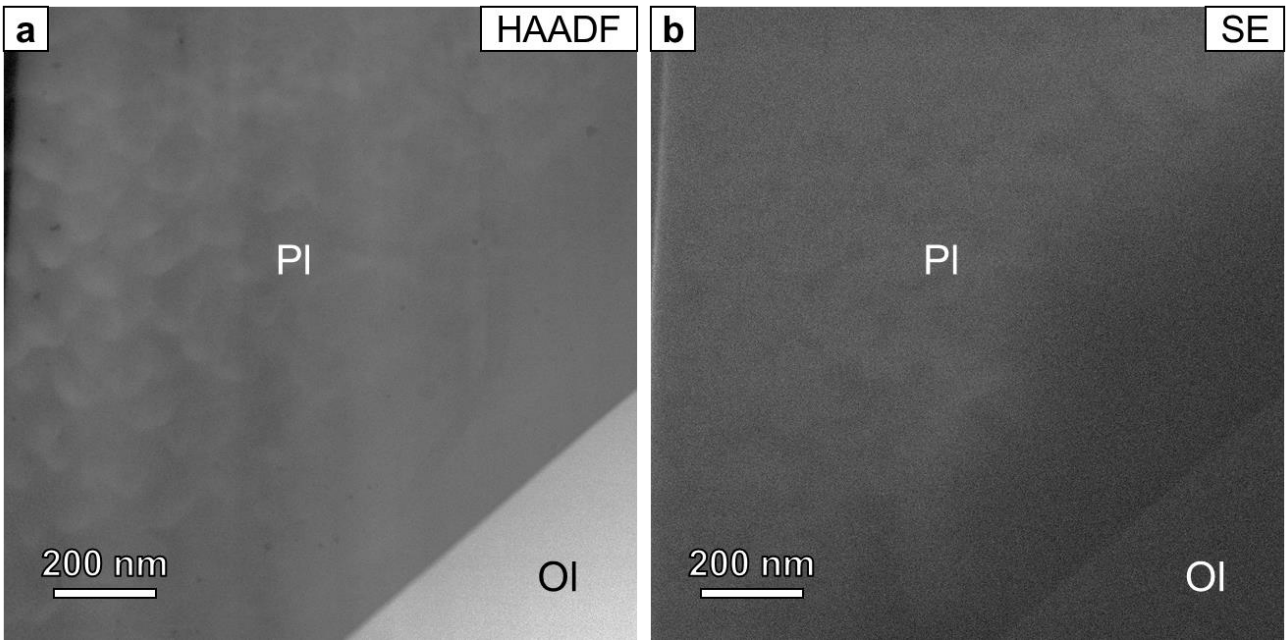

Supplementary Fig. 10 | HAADF and SE images of FIB section #4 after re-thinning. All the NaCl grains previously present on the surface of plagioclase (Pl) are removed. No NaCl inclusions are found. Additional abbreviation: Ol, olivine.

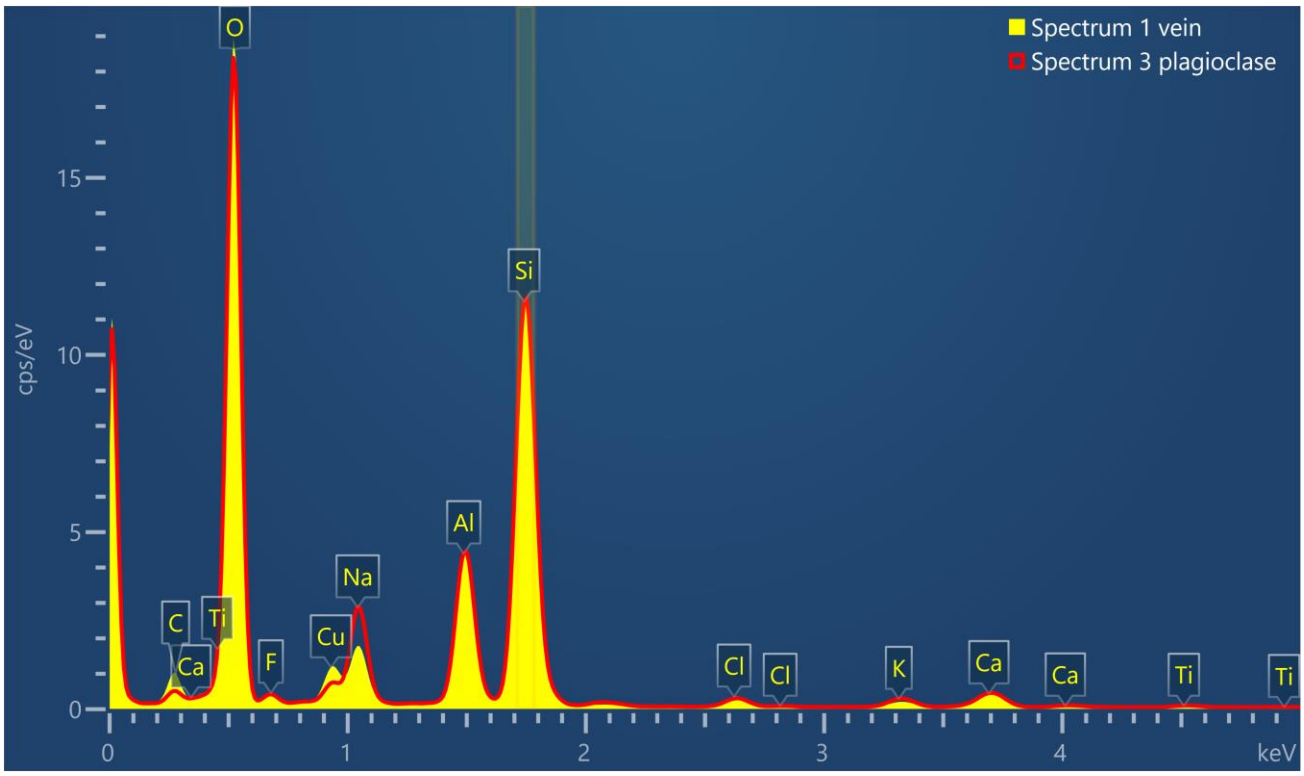

Supplementary Fig. 11 | Comparison of EDS spectra of the vein (yellow) and plagioclase (red) in FIB section #5. Both spectra are normalized to the Si Kα peak to eliminate the thickness effect. The vein has a similar composition to plagioclase, but is significantly depleted in Na.

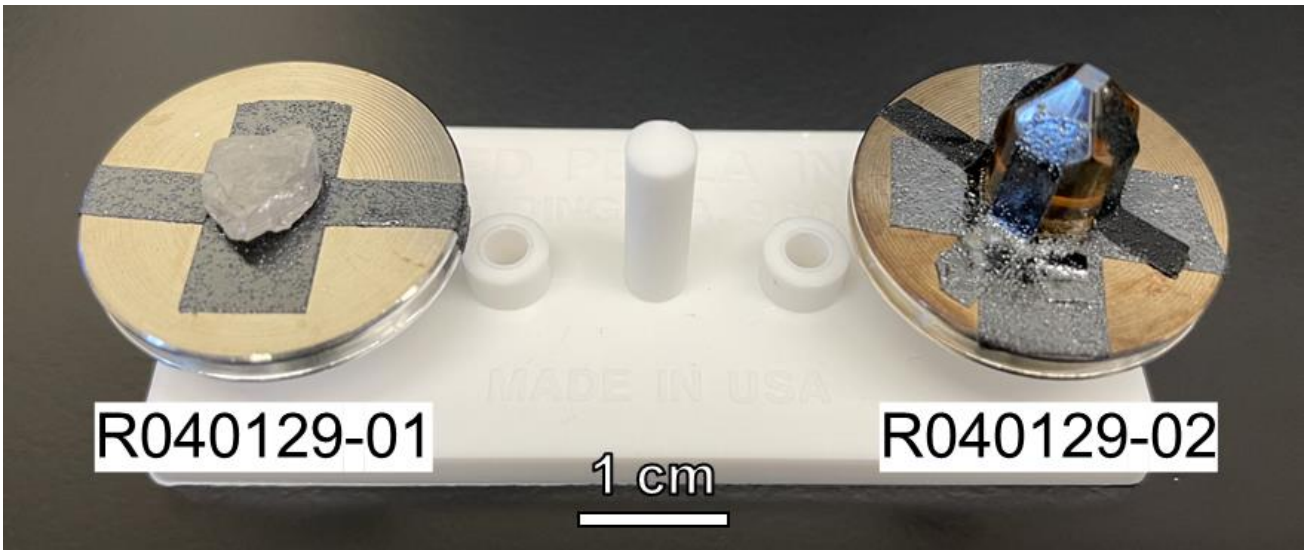

Supplementary Fig. 12 | The two fragments of the R040129 albite sample sitting on the SEM pin mounts. The albite fragment on the left (R040129-01) was directly placed on the holder, with a flat cleavage plane facing upwards. The other fragment shown on the right (R040129-02) was first embedded in an epoxy bullet and subsequently sliced to expose a flat surface of albite. Both fragments were carbon coated prior to imaging on the Helios FIB-SEM.

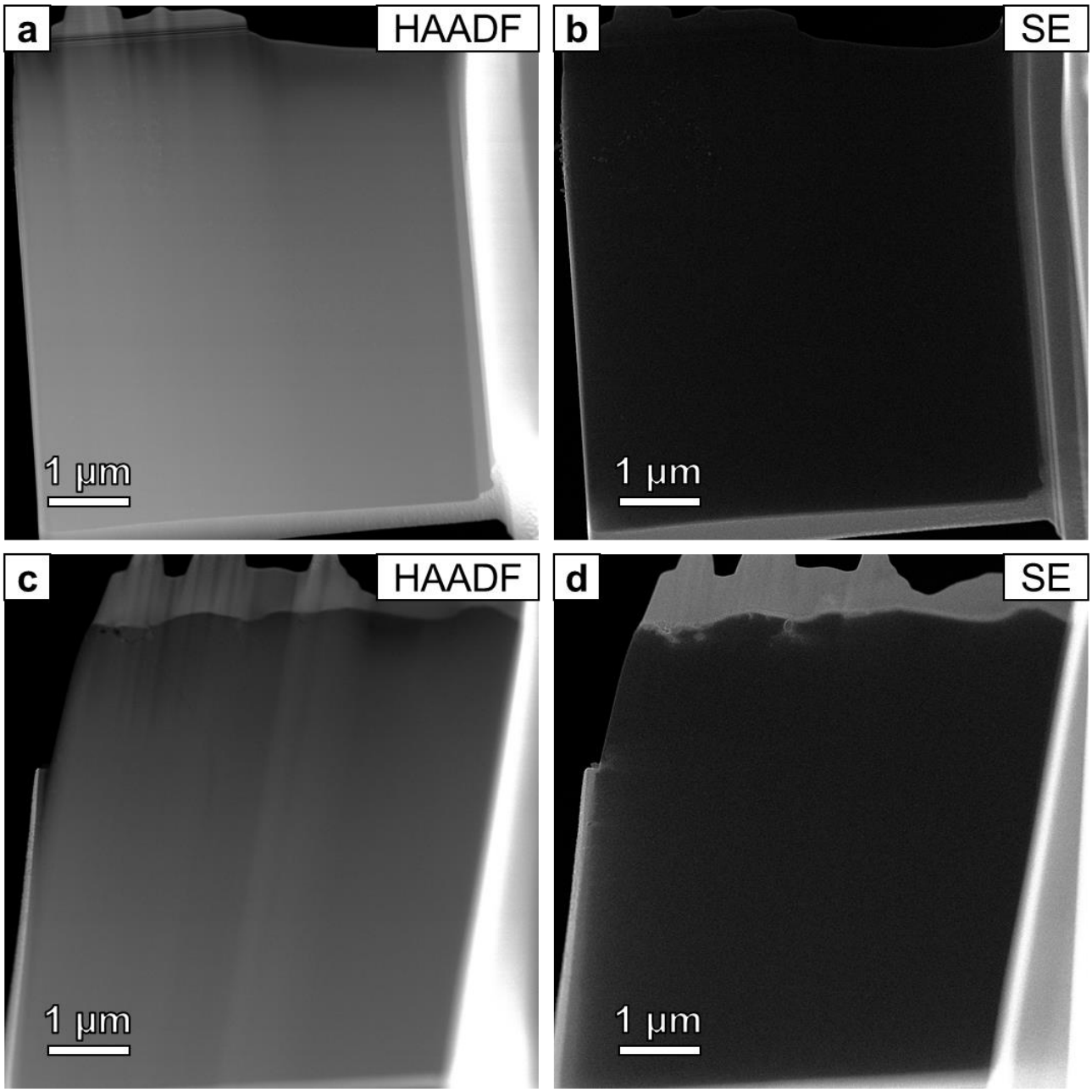

Supplementary Fig. 13 | STEM images of FIB sections extracted from R040129-01 (a-b) and -02 (c-d), respectively. Both sections are featureless and do not contain any surface adhering grains.

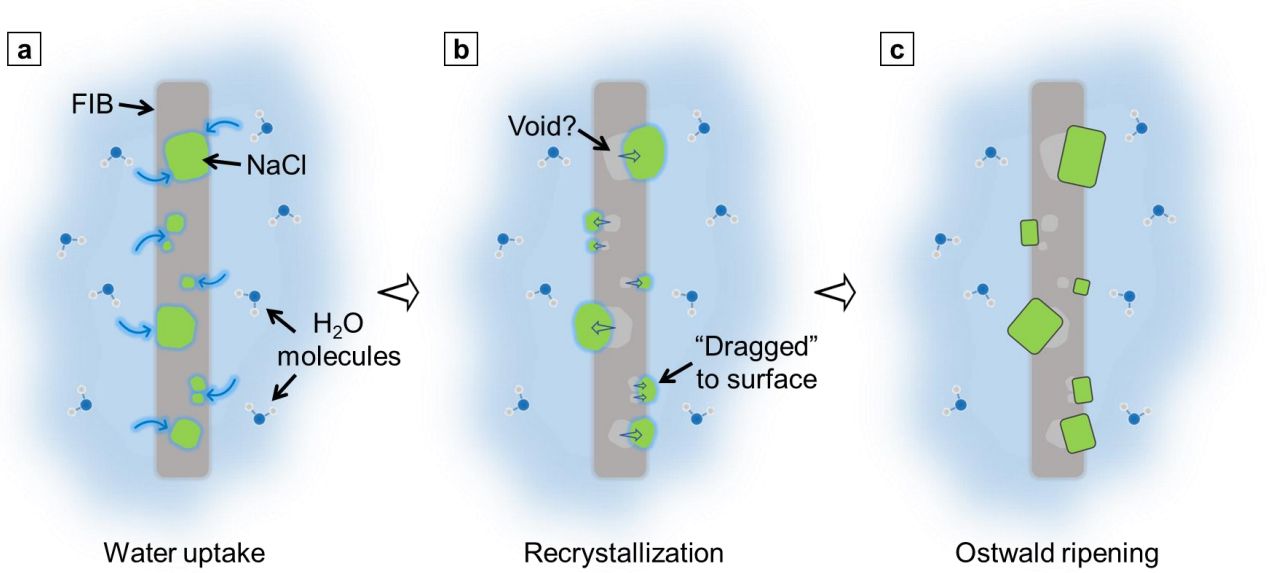

Supplementary Fig. 14 | A cartoon schematic illustrating the migration process of NaCl inclusions to the FIB section surfaces. The FIB section in the figure is viewed edge on. (**a**) NaCl inclusions gradually absorb ambient water molecules during storage in the desiccator. (**b**) NaCl grains partially dissolve into the water monolayers and subsequently recrystallize on the surfaces of the FIB section. The inclusions being "dragged" to the surfaces could have left voids in the section. (**c**) After migrating to the surfaces, NaCl grains continued to interact with moisture, resulting in grain coarsening and more euhedral shapes, which was driven by Ostwald ripening.

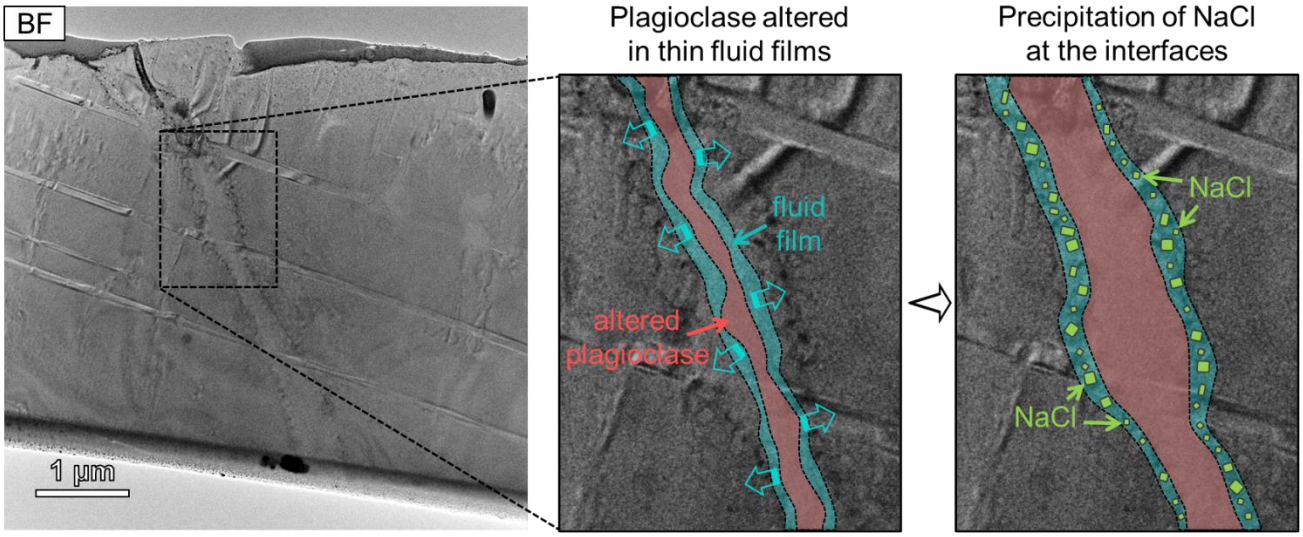

Supplementary Fig. 15 | TEM data and schematic diagram for the formation process of the alteration vein in FIB section #5. A late-stage fluid penetrated into plagioclase through a fracture. Plagioclase was gradually dissolved at the reaction front in the thin fluid film. A metastable phase with a similar composition to plagioclase but depleted in Na formed as a transient alteration product. As the fluid front migrated towards the unaltered plagioclase, the alteration vein grew increasingly wider. NaCl eventually precipitated at the alteration interfaces at a late stage when the fluid composition became extremely NaCl-rich.

Supplementary Tables 1 and 2

Supplementary Table 1 | STEM EDS compositions of the vein in FIB section #5.

	Vein Spectrum 1			Vein Spectrum 2			Vein Spectrum 3			Vein Spectrum 4			Vein Spectrum 5			Vein Spectrum 6		
Element	Wt%	Wt% σ	Number of Ions	Wt%	Wt% σ	Number of Ions	Wt%	Wt% σ	Number of Ions	Wt%	Wt% σ	Number of Ions	Wt%	Wt% σ	Number of Ions	Wt%	Wt% σ	Number of Ions
O	49.59	0.21	8.00	49.90	0.21	8.00	49.87	0.21	8.00	49.45	0.23	8.00	49.85	0.26	8.00	49.41	0.20	8.00
Na	3.96	0.07	0.44	3.31	0.07	0.37	3.41	0.07	0.38	4.47	0.08	0.50	3.46	0.08	0.39	4.49	0.07	0.51
Al	11.35	0.11	1.09	11.27	0.11	1.07	11.23	0.11	1.07	11.07	0.12	1.06	11.31	0.13	1.08	11.18	0.10	1.07
Si	32.67	0.16	3.00	33.23	0.16	3.03	33.19	0.16	3.03	32.61	0.17	3.01	33.13	0.20	3.03	32.49	0.15	3.00
K	0.63	0.03	0.04	0.54	0.03	0.04	0.51	0.03	0.03	0.64	0.03	0.04	0.56	0.03	0.04	0.68	0.03	0.05
Ca	1.59	0.04	0.10	1.53	0.04	0.10	1.58	0.04	0.10	1.54	0.04	0.10	1.48	0.05	0.09	1.53	0.04	0.10
Ti	0.21	0.03	0.01	0.23	0.03	0.01	0.23	0.03	0.01	0.23	0.03	0.01	0.20	0.03	0.01	0.21	0.03	0.01
Total	100.00			100.00			100.00			100.00			100.00			100.00		
Na,K,Ca sum			0.58			0.51			0.51			0.64			0.52			0.66
Average (Na,K,Ca sum)			0.57															

Supplementary Table 2 | STEM EDS compositions of the plagioclase in FIB section #5.

	Plagioclase Spectrum 1			Plagioclase Spectrum 2			Plagioclase Spectrum 3			Plagioclase Spectrum 4			Plagioclase Spectrum 5			Plagioclase Spectrum 6		
Element	Wt%	Wt% σ	Number of Ions	Wt%	Wt% σ	Number of Ions	Wt%	Wt% σ	Number of Ions	Wt%	Wt% σ	Number of Ions	Wt%	Wt% σ	Number of Ions	Wt%	Wt% σ	Number of Ions
O	48.78	0.20	8.00	48.92	0.30	8.00	49.02	0.19	8.00	48.75	0.21	8.00	48.81	0.19	8.00	48.73	0.25	8.00
Na	6.30	0.07	0.72	5.98	0.11	0.68	5.43	0.07	0.62	6.11	0.08	0.70	5.99	0.07	0.68	6.25	0.09	0.71
Al	10.91	0.10	1.06	10.81	0.15	1.05	11.04	0.10	1.07	11.08	0.11	1.08	10.97	0.10	1.07	10.91	0.12	1.06
Si	31.59	0.15	2.95	31.91	0.23	2.97	31.93	0.14	2.97	31.47	0.15	2.94	31.65	0.14	2.95	31.53	0.18	2.95
K	0.68	0.03	0.05	0.70	0.04	0.05	0.82	0.03	0.05	0.87	0.03	0.06	0.86	0.03	0.06	0.87	0.04	0.06
Ca	1.53	0.03	0.10	1.45	0.05	0.09	1.56	0.03	0.10	1.50	0.04	0.10	1.53	0.03	0.10	1.48	0.04	0.10
Ti	0.21	0.02	0.01	0.23	0.04	0.01	0.19	0.02	0.01	0.21	0.03	0.01	0.19	0.02	0.01	0.24	0.03	0.01
Total	100.00			100.00			100.00			100.00			100.00			100.00		
Na,K,Ca sum			0.87			0.82			0.77			0.86			0.84			0.87
Average (Na,K,Ca sum)			0.84															

Supplementary References

51. Klein, C., Dutrow, B., Dana, J. D. & Klein, C. *Manual of mineral science*. (Wiley New York, 2002).
52. Brearley, A. J. & Krot, A. N. Metasomatism in the early solar system: The record from chondritic meteorites. in *Metasomatism and the chemical transformation of rock* (eds. Harlov, D. E. & Austrheim, A.) vol. 56 659–789 (Springer, Berlin Heidelberg, 2013).
53. Brearley, A. J. & Jones, R. H. Halogens in chondritic meteorites. in *The Role of Halogens in Terrestrial and Extraterrestrial Geochemical Processes* (eds. Harlov, D. E. & Aranovich, L.) 871–958 (Springer, Cham, 2018). doi:10.1007/978-3-319-61667-4_15.
54. Lewis, J. A., Jones, R. H. & Brearley, A. J. Plagioclase alteration and equilibration in ordinary chondrites: 5Metasomatism during thermal metamorphism. *Geochim. Cosmochim. Acta* **316**, 201–229 (2022).
55. Putnis, A. Mineral replacement reactions. *Rev. Mineral. Geochemistry* **70**, 87–124 (2009).
56. Engvik, A. K., Putnis, A., Fitz Gerald, J. D. & Austrheim, H. Albitization of granitic rocks: The mechanism of replacement of oligoclase by albite. *Can. Mineral.* **46**, 1401–1415 (2008).
57. Krot, A. N., Petaev, M. I. & Nagashima, K. Infiltration metasomatism of the Allende coarse-grained calcium-aluminum-rich inclusions. *Prog. Earth Planet. Sci.* **8**, 61 (2021).
58. Stoffler, D., Bischoff, A., Buchwald, V. & Rubin, A. E. Shock effects in meteorites. *Meteorites early Sol. Syst.* 165–202 (1988).
59. Rubin, A. E., Scott, E. R. D. & Keil, K. Shock metamorphism of enstatite chondrites. *Geochim. Cosmochim. Acta* **61**, 847–858 (1997).
60. Suttle, M. D., King, A. J., Schofield, P. F., Bates, H. & Russell, S. S. The aqueous alteration of CM chondrites, a review. *Geochim. Cosmochim. Acta* **299**, 219–256 (2021).
61. Lee, M. R., Lindgren, P. & Sofe, M. R. Aragonite, breunnerite, calcite and dolomite in the CM carbonaceous chondrites: High fidelity recorders of progressive parent body aqueous alteration. *Geochim. Cosmochim. Acta* **144**, 126–156 (2014).
62. Ruiz-Agudo, E., Putnis, C. V. & Putnis, A. Coupled dissolution and precipitation at mineral-fluid interfaces. *Chem. Geol.* **383**, 132–146 (2014).
63. Perdikouri, C., Piazolo, S., Kasioptas, A., Schmidt, B. C. & Putnis, A. Hydrothermal replacement of Aragonite by Calcite: Interplay between replacement, fracturing and growth. *Eur. J. Mineral.* **25**, 123–136 (2013).
64. Putnis, A. Fluid–mineral interactions: Controlling coupled mechanisms of reaction, mass transfer and deformation. *J. Petrol.* **62**, 1–27 (2021).
65. Putnis, A. & Austrheim, H. Fluid-induced processes: Metasomatism and metamorphism. *Geofluids* **10**, 254–269 (2010).
66. Putnis, A. Transient porosity resulting from fluid–mineral interaction and its consequences. *Rev. Mineral. Geochemistry* **80**, 1–23 (2015).
67. Zolensky, M. E. *et al.* The search for and analysis of direct samples of early Solar System aqueous fluids. *Philos. Trans. R. Soc. A Math. Phys. Eng. Sci.* **375**, (2017).
68. Tsuchiyama, A. *et al.* Discovery of primitive CO_2-bearing fluid in an aqueously altered carbonaceous chondrite. *Sci. Adv.* **7**, eabg9707 (2021).
69. Zolensky, M. E. *et al.* Asteroidal water within fluid inclusion-bearing halite in an H5 chondrite, Monahans (1998). *Science* **285**, 1377–1379 (1999).
70. Rubin, A. E., Zolensky, M. E. & Bodnar, R. J. The halite-bearing Zag and Monahans (1998) meteorite breccias: Shock metamorphism, thermal metamorphism and aqueous alteration on the H-chondrite

parent body. *Meteorit. Planet. Sci.* **37**, 125–141 (2002).
71. Whitby, J., Burgess, R., Turner, G., Gilmour, J. & Bridges, J. Extinct ^{129}I in halite from a primitive meteorite: Evidence for evaporite formation in the early solar system. *Science* **288**, 1819–1821 (2000).
72. Tartèse, R., Hull, R. & Jones, R. H. U-Pb dating and REE systematics of phosphate minerals in the H4 and H6 lithologies of the Zag chondrite. *Annu. Meet. Meteorit. Soc.* **85**, 6257 (2022).
73. Zolotov, M. Y. & Mironenko, M. V. Hydrogen chloride as a source of acid fluids in parent bodies of chondrites. *Lunar Planet. Sci.* **38**, 2340 (2007).
74. Bland, P. A. *et al.* Why aqueous alteration in asteroids was isochemical: High porosity ≠ high permeability. *Earth Planet. Sci. Lett.* **287**, 559–568 (2009).
75. Jones, R. H. *et al.* Phosphate minerals in LL chondrites: A record of the action of fluids during metamorphism on ordinary chondrite parent bodies. *Geochim. Cosmochim. Acta* **132**, 120–140 (2014).
76. Jones, R. H., Mccubbin, F. M. & Guan, Y. Phosphate minerals in the H group of ordinary chondrites, and fluid activity recorded by apatite heterogeneity in the Zag H3-6 regolith breccia. *Am. Mineral.* **101**, 2452–2467 (2016).
77. Elkins-Tanton, L. T., Weiss, B. P. & Zuber, M. T. Chondrites as samples of differentiated planetesimals. *Earth Planet. Sci. Lett.* **305**, 1–10 (2011).
78. Weiss, B. P. *et al.* Possible evidence for partial differentiation of asteroid Lutetia from Rosetta. *Planet. Space Sci.* **66**, 137–146 (2012).
79. Šrámek, O., Milelli, L., Ricard, Y. & Labrosse, S. Thermal evolution and differentiation of planetesimals and planetary embryos. *Icarus* **217**, 339–354 (2012).
80. Fu, R. R. & Elkins-Tanton, L. T. The fate of magmas in planetesimals and the retention of primitive chondritic crusts. *Earth Planet. Sci. Lett.* **390**, 128–137 (2014).
81. Ganino, C. & Libourel, G. Reduced and unstratified crust in CV chondrite parent body. *Nat. Commun.* **8**, (2017).
82. Lewis, J. A. & Jones, R. H. Phosphate and feldspar mineralogy of equilibrated L chondrites: The record of metasomatism during metamorphism in ordinary chondrite parent bodies. *Meteorit. Planet. Sci.* **51**, 1886–1913 (2016).
83. Lewis, J. A. & Jones, R. H. Exsolution in alkali feldspar in ordinary chondrites: Ubiquitous evidence for rapid cooling at high temperatures. *Geochim. Cosmochim. Acta* **321**, 293–310 (2022).
84. Brady, J. B. & Yund, R. A. Interdiffusion of K and Na in alkali feldspars: Homogenization experiments. *Am. Mineral.* **68**, 106–111 (1983).
85. Cherniak, D. J. Cation diffusion in feldspars. *Rev. Mineral. Geochemistry* **72**, 691–733 (2010).
86. Bridges, J. C., Banks, D. A., Smith, M. & Grady, M. M. Halite and stable chlorine isotopes in the Zag H3-6 breccia. *Meteorit. Planet. Sci.* **39**, 657–666 (2004).
87. Fries, M., Messenger, S., Steele, A. & Zolensky, M. The H chondrite halite parent body: Warm, wet, organic-rich, rather habitable and possibly Ceres. *Work. Habitability Icy Worlds* 4078 (2014).
88. Yurimoto, H. *et al.* Isotopic compositions of asteroidal liquid water trapped in fluid inclusions of chondrites. *Geochem. J.* **48**, 549–560 (2014).
89. Perez, R. J. & Boles, J. R. An empirically derived kinetic model for albitization of detrital plagioclase. *Am. J. Sci.* **305**, 312–343 (2005).
90. Beitter, T., Wagner, T. & Markl, G. Formation of kyanite-quartz veins of the Alpe Sponda, Central Alps, Switzerland: Implications for Al transport during regional metamorphism. *Contrib. to Mineral. Petrol.* **156**, 689–707 (2008).
91. Zolotov, M. Y., Mironenko, M. V. & Shock, E. L. Thermodynamic constraints on fayalite formation on

parent bodies of chondrites. *Meteorit. Planet. Sci.* **41**, 1775–1796 (2006).
92. Jin, Z. & Bose, M. New clues to ancient water on Itokawa. *Sci. Adv.* **5**, 1–10 (2019).
93. Alexander, C. M. O. *et al.* The provenances of asteroids, and their contributions to the volatile inventories of the terrestrial planets. *Science* **337**, 721–723 (2012).
94. Alexander, C. M. O., McKeegan, K. D. & Altwegg, K. Water reservoirs in small planetary bodies: Meteorites, asteroids, and comets. *Space Sci. Rev.* **214**, 36 (2018).
95. Vacher, L. G. *et al.* Hydrogen in chondrites: Influence of parent body alteration and atmospheric contamination on primordial components. *Geochim. Cosmochim. Acta* **281**, 53–66 (2020).
96. Grant, H., Tartèse, R., Jones, R. H., Marrocchi, Y. & Piani, L. Bulk water abundances and D/H ratios of unequilibrated ordinary chondrites. *Lunar Planet. Sci.* **52**, 2242 (2021).
97. Lewis, J. A., Jones, R. H. & Garcea, S. C. Chondrule porosity in the L4 chondrite Saratov: Dissolution, chemical transport, and fluid flow. *Geochim. Cosmochim. Acta* **240**, 293–313 (2018).
98. Kovach, H. A. & Jones, R. H. Feldspar in type 4-6 ordinary chondrites: Metamorphic processing on the H and LL chondrite parent bodies. *Meteorit. Planet. Sci.* **45**, 246–264 (2010).
99. Krumgalz, B. S. Temperature dependence of mineral solubility in water. Part I. Alkaline and alkaline earth chlorides. *J. Phys. Chem. Ref. Data* **46**, 043101 (2017).